NMR Dynamics Investigation of Ligand Induced Changes of Main and Side Chain Arginine N-H's in Human Phosphomevalonate Kinase

Andrew L. Olson, Sheng Cai, Timothy J. Herdendorf, Henry M. Miziorko, and Daniel S. Sem*

Chemical Proteomics Facility at Marquette, Department of Chemistry, Marquette University, P.O. Box 1881, Milwaukee, Wisconsin 53201and Division of Molecular Biology and Biochemistry, School of Biological Sciences, University of Missouri-Kansas City, Kansas City, Missouri 64110.

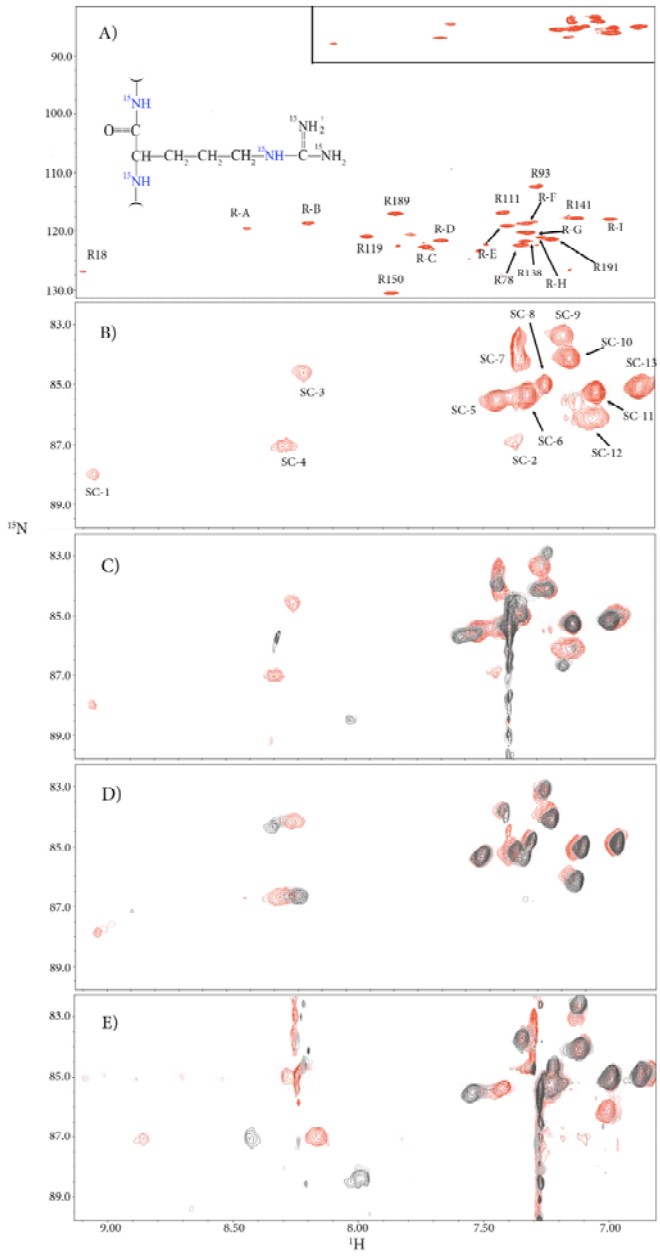

Figure S1. Arg-PMK chemical shifts, including side chains (top) and backbone (bottom). (B) Expanded region of side chain chemical shifts. (C) Chemical shift titration showing increasing amounts (100 uM increments) of M5P added to apo-PMK (red) to saturation (1 mM) shown in gray. (D) Chemical shift titration of increasing amounts of MgADP added to apo-PMK (red) to saturation (1 mM), shown in gray. (E) Chemical shift titration of increasing amounts of M5P added to the MgADP/PMK complex (red), forming the ternary complex (1 mM) shown in gray. Backbone and sidechain ^{15}N-H atoms, monitored in the spectra, are identified on the arginine structure (blue) shown in the inset in panel B, although the ε-N-H is the only observable sidechain NH, since it is the least acidic (least prone to exchange with solvent). Spectra were taken at 600 MHz at 298 K. Arginine backbone assignments are indicated, when available. SC-1 to SC-13 are unassigned arginine side chain N-H's (no side chains have been assigned). R-A to R-I are unassigned arginine backbone N-H's.

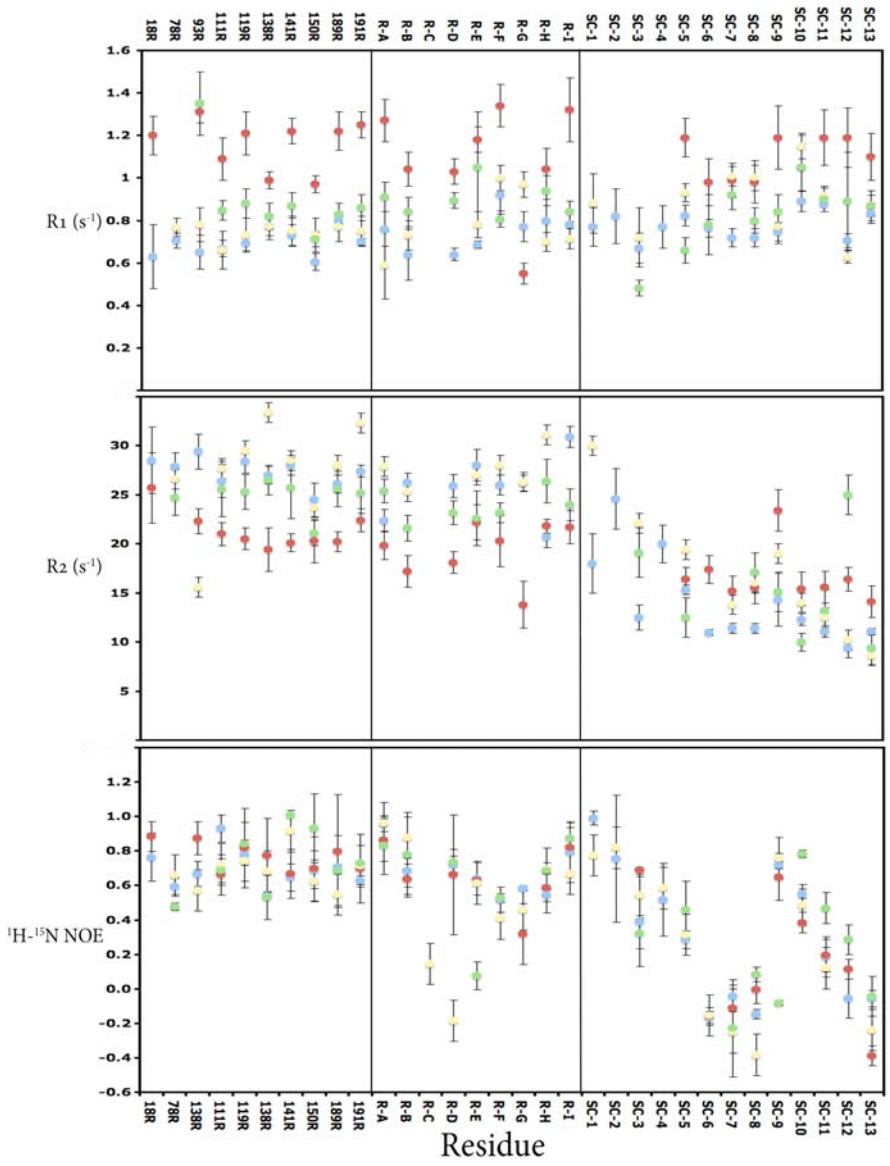

Figure S2. NMR dynamics data including R_1, R_2, and ^1H-^{15}N NOE values, where blue is apo-PMK, red is the M5P/PMK binary complex, yellow is the MgADP/PMK binary complex, and green is the M5P/MgADP/PMK ternary complex. The sections are divided into assigned backbone N-H's, unassigned backbone N-H's and side chain guanido N-H's. These are the data that were used to calculate order parameters in Figure 3.

	Free	M5P	MgADP	MgADP/M5P
R_1 (s^{-1})	0.78 ± 0.06	1.1 ± 0.13	0.89 ± 0.07	0.82 ± 0.09
R_2 (s^{-1})	14.0 ± 1.3	16.6 ± 1.5	16.6 ± 2.1	15.2 ± 1.9
^{1}H-^{15}N NOE	0.30 ± 0.11	0.15 ± 0.08	0.28 ± 0.10	0.23 ± 0.11
S^2	0.47 ± 0.04	0.67 ± 0.09	0.64 ± 0.04	0.75 ± 0.06
τ_c (ns)	20.1	15.5	22.0	18.4

Table S1. Average dynamic parameters for the ε-NH's of arginine sidechains, with the correlation time (τ_c) of the backbone arginine residues used for calculating S^2 values of the arginine sidechain N-H's. Note: These are only averaged in those cases where all four complexes have data for a particular sidechain residue.

Residue Number	**Tentative Assignment**	**Distance to Nearest Neg. Charge (ε-NH)**		**S^2 Values of PMK Complexes**			
		Distance	**Atom**	**Apo**	**M5P**	**ADP**	**Ternary**
SC-3	R84	3.0 Å	Carboxyl of M5P	0.588	-----	0.875	0.648
SC-4	R111	2.6 Å	Carboxyl of M5P	0.593	-----	-----	-----
SC-5	R130	14 Å	γ-phosphate of ATP	0.417	0.618	0.730	0.734
SC-12	R141	14 Å	α-phosphate of ATP	0.418	0.597	0.667	0.802

Table S2. Distance from arginine sidechain NH (for those that were tentatively assigned using site-directed mutagenesis) to the nearest negatively charged atom on either substrate. Also shown are changes in order parameter, when available. Note that while R141 is close to substrate, it is still distal from any charged atom on the substrate.

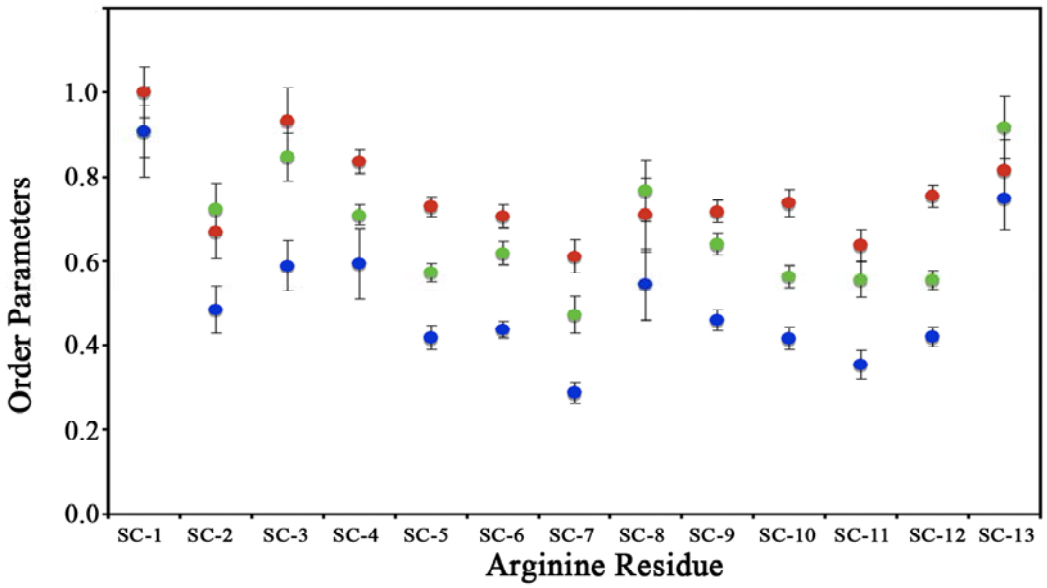

Figure S3. Plot of apo-PMK modelfree S^2 results which fit to model 5, where blue is the resulting generalized order parameter (S^2) from S^2_f (red) and S^2_s (green).

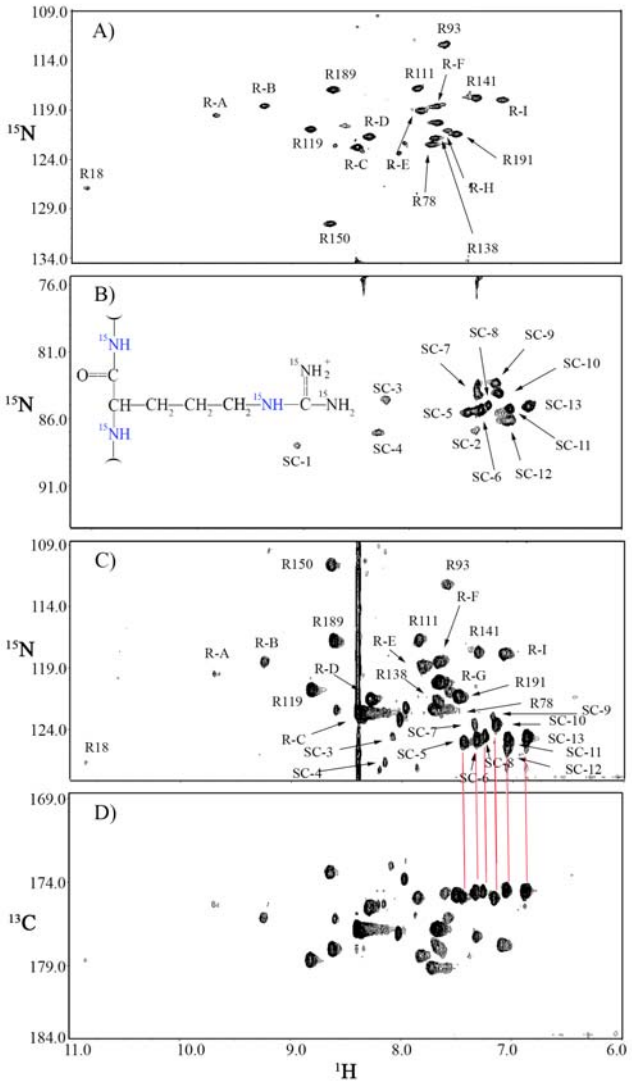

Figure S4. HNCO and HSQC spectra of ^{15}N/^{13}C-Arg and U-^{13}C PMK. Spectra are of PMK that is uniformly ^{13}C labeled, and has ^{15}N label present only in arginines. Spectra in panels (A) and (B) are standard ^{1}H-^{15}N HSQC spectra, of backbone and sidechain regions of ^{15}N-Arg labeled PMK, and are provided for comparison with HNCO 2D planes (panels (C) and (D)). The ^{1}H-^{15}N plane from the 3D HNCO spectrum (panel (C)) shows crosspeaks for arginine backbone ^{15}NH's, adjacent to ^{13}C=O carbonyls, but also for arginine sidechain ^{15}NHε's, adjacent to ^{13}C=NH$_2$ iminos, of the guanidinium groups. Panel (D) shows the corresponding ^{1}H-^{13}C HNCO plane, that correlates proton shift of the arginine backbone or epsilon ^{15}NH with ^{13}C chemical shift of the adjacent carbonyl or imino carbon. Imino ^{13}Cζ shifts are identified with red lines. In panel (C), the R150 backbone and all NHε sidechain crosspeaks are folded, as are the sidechain ^{13}Cζ crosspeaks in panel (D).

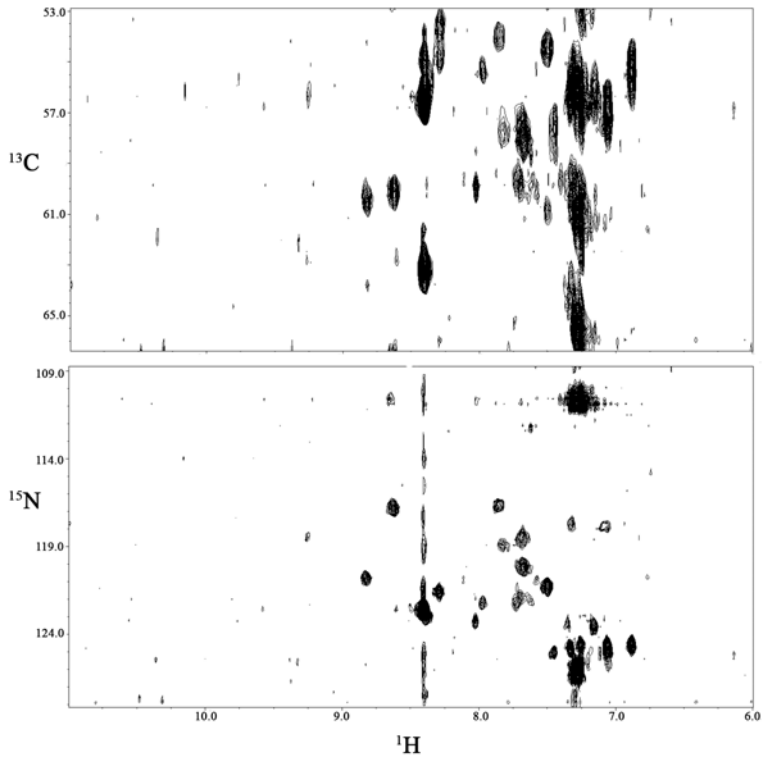

Figure S5. HNCA of ^{15}N/^{13}C-Arg and U-^{13}C PMK. Spectra are of PMK that is uniformly ^{13}C labeled, and has ^{15}N label present only in arginines. Spectra are 2D ^{1}H-^{13}C (top) and ^{1}H-^{15}N (bottom) planes from the 3D HNCA experiment. These spectra provide confirmation for arginine specific labeling, versus scrambling of label. Sidechain crosspeaks show connection of the NHε proton to the CHδ of the sidechain. An HNCACB was also performed, but gave little signal.

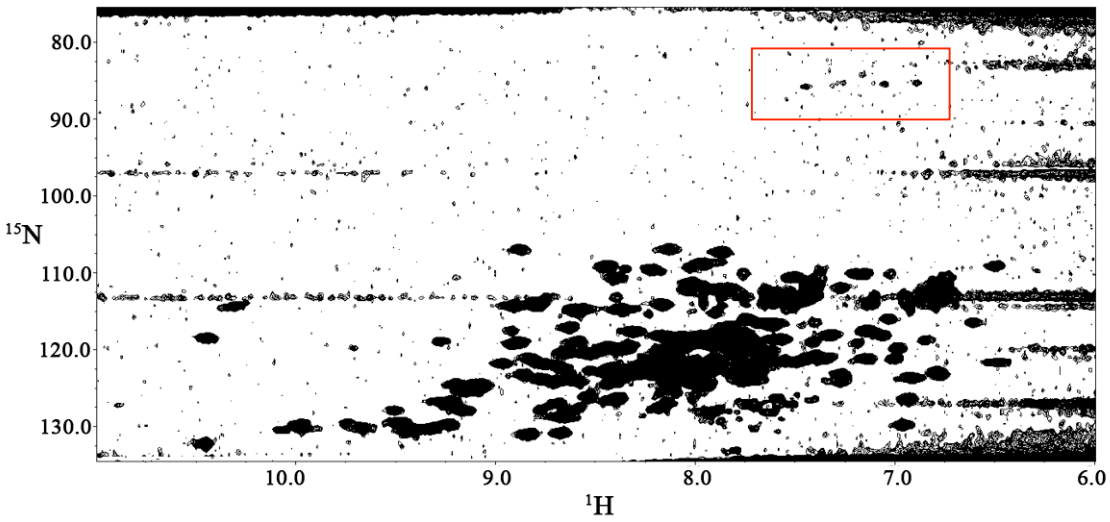

Figure S6. ^{15}N-^{1}H plane from a ^{15}N-NOESY experiment of 500 uM apo-PMK in 20 mM potassium phosphate at pH 6.5. ^{15}N-NOESY was run with mixing times of 80 and 150 ms, ε-NH signal was weak (shown in red box) compared to backbone NH's, due to increased exchange with water. These data are shown, to demonstrate the infeasibility of arginine sidechain assignment using the NOESY experiment. Similar problems were encountered with TOCSY experiments as well.

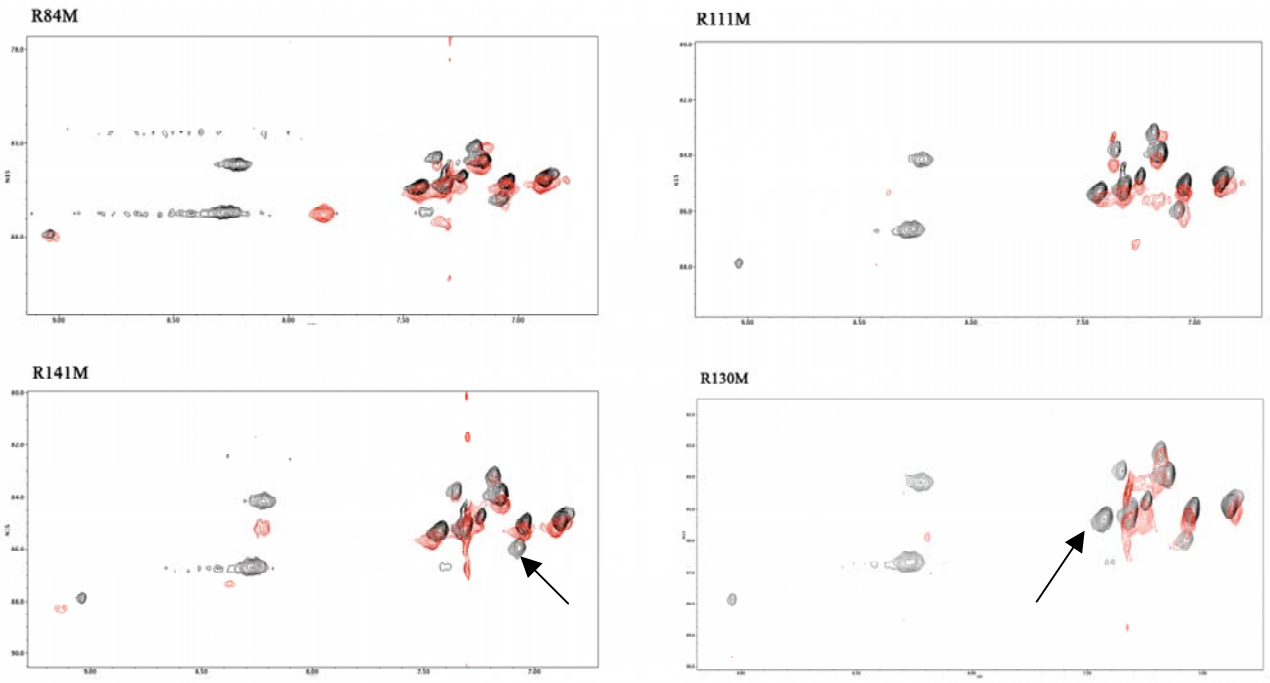

Figure S7. Assignment by site-directed mutagenesis. ^{1}H-^{15}N HSQC spectra of the arginine ε-NH region where black indicates apo-PMK arginine chemical shifts, and red is for mutant (R84M, R141M, R111M, and R130M) PMK chemical shifts. In the R84M and R111M panels, notice that mutation causes the 3 crosspeaks on the left to be perturbed, either broadening or shifting, suggesting that these arginine sidechains are likely to be in some proximity to each other. This is consistent with our earlier M5P titration (Figure S1), that showed these same 3 cross peaks broaden upon binding. The R141M mutant causes some cross peaks to change slightly, however one crosspeak (SC-12) clearly disappears, suggesting it is most likely for the ε-NH of R141. As with the R141M mutant, the R130M mutant causes cross peaks to change slightly, however SC-5 completely disappears, implying this is probably the ε-NH of R130.

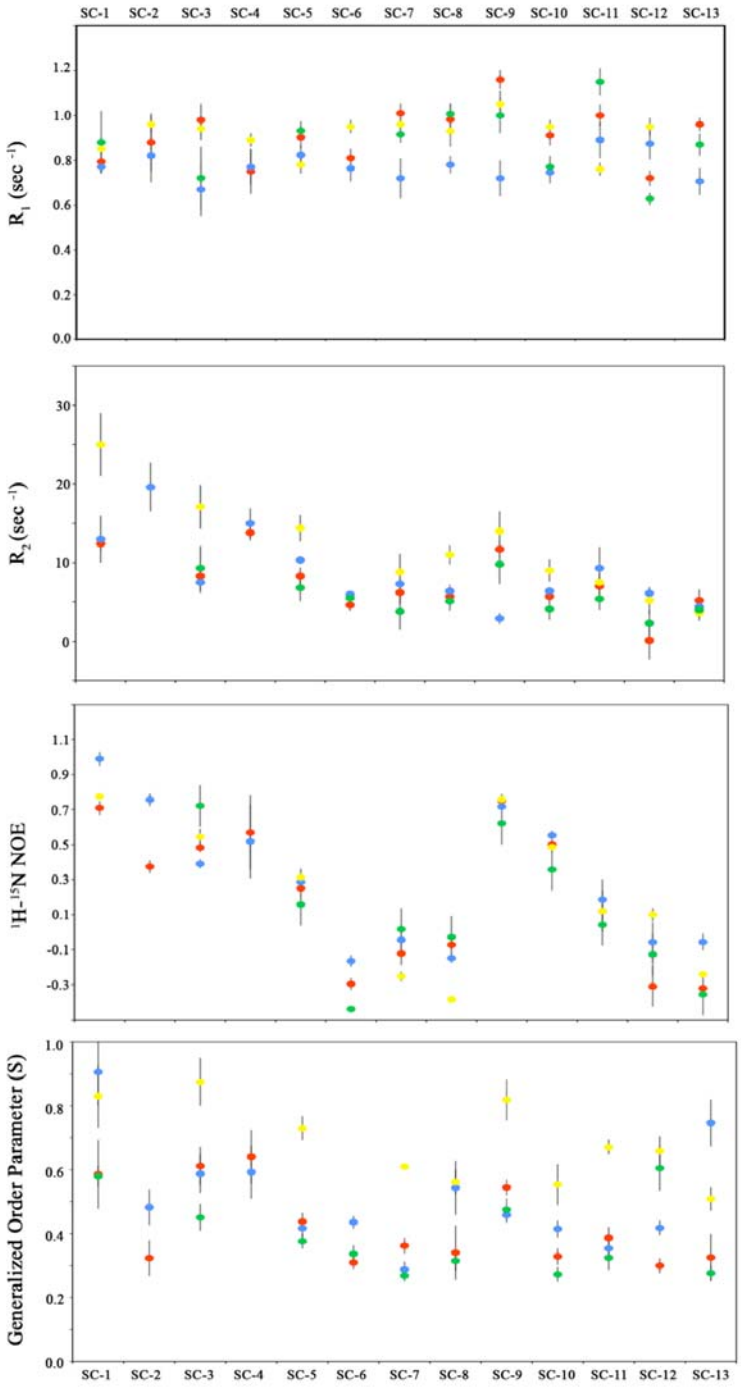

Figure S8. Effect of adding 100 mM KCl. NMR dynamics data of arginine side chain ε-NH's of PMK including the $R_1$and R_2 relaxation rates, ^{1}H-^{15}N NOE, and the generalized order parameter (S^2), where blue is Apo PMK, red is Apo PMK in NMR buffer including 100 mM KCl, yellow is MgADP bound PMK, and green is MgADP bound PMK in NMR buffer including 100 mM KCl. Addition of KCl into the buffer causes the R_2 values the MgADP bound PMK to decrease on average from 15 sec^{-1} to 10 sec^{-1} which subsequently seems to cause the S^2 values to decrease in every arginine NH (except SC-12/R141). It should be noted that MgADP bound PMK without buffer was able to fit to model 4 while addition of salt seemed to cause the dynamical changes to fit only model 5. It should also be noted that the backbone NH's of MgADP bound PMK with KCl buffer behaved the exact same way as with regular NMR buffer, suggesting that only the ε-NH's are only effected by the ionic interactions with salt.

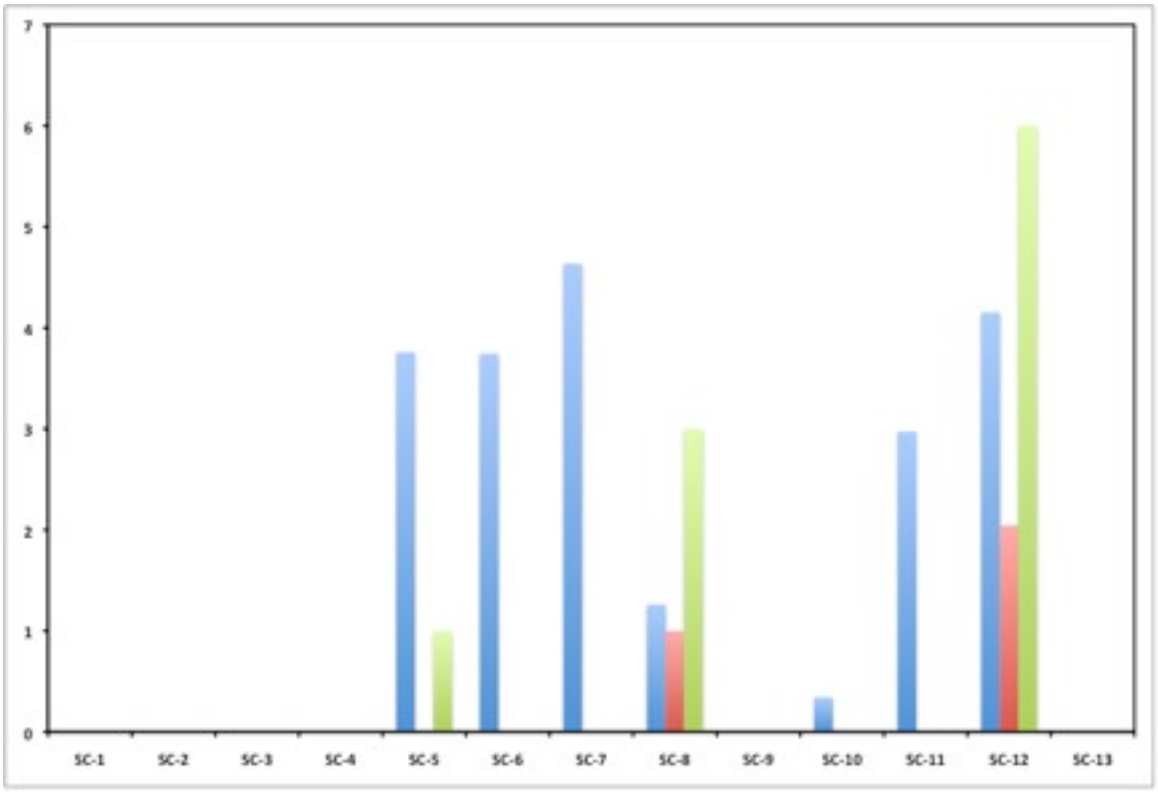

Figure S9. Rex terms that resulted from fitting of NMR dynamics data (R1, R2, NOE) to Model 4, for: M5P-PMK (blue), ADP-PMK (red), M5P-ADP-PMK ternary complex (green).

Methods and Materials

Docking of M5P and ATP into Human PMK Crystal Structure

The binding orientation of ligands in the PMK (human) crystal structure (3CH4) was calculated using Autodock4.[14] Gasteiger charges and hydrogens were added using AutoDock Tools (ADT). The docking grids were also prepared using ADT, with a grid size of 60 x 60 x 60 Å and a spacing of 0.375 Å. These grids were centered on the ligands (AMP and GMP) of the homologous protein, bacteriophage T4 deoxynucleotide kinase.[15] The PMK crystal structure (apo) and template were superimposed on each

other, to determine coordinates for the grid box used to dock ligands. Default docking parameters were used, except 50 genetic algorithm runs were used with 2,500,000 for maximum number of evaluations. The docking of both ligands was done separately, due to inter-ligand repulsion from the negative charges on M5P and the ATP triphosphate, even after neutralization of two ATP charges (as would be the case with bound Mg^{2+}). This repulsive interaction was recognized based on earlier docking attempts to form the ternary complex, which produced distorted structures with the phosphate groups on the two ligands as far apart as possible. This led us to do independent docking of ATP and M5P to produce the separate binary complexes, and these pdb coordinate files were then merged to create the ternary complex. The crystal structure of PMK has the R141 positioned in the proposed binding site of ATP, so that docking of ATP into that site caused the ATP to adopt a highly strained conformation with a steric clash involving R141. So to achieve a proper docking, with minimal perturbation to the crystal structure, R141 was temporality changed to glycine. This allowed a proper docking of ATP into the active site. Then the R141 sidechain was added back and, as expected, there was still a steric clash with the R141 sidechain and ATP. This merged ATP/PMK pdb file was then minimized using Amber 99, as implemented by HyperChem 7.5 (Gainesville, FL). The minimized structure was then further refined by performing a brief molecular dynamics (MD) run (again using the Amber 99 force field, as implemented in HyperChem 7.5) to determine any lid motion that may be required to permit ATP binding. MD was performed using a 1 fsec step size, with a heating time of 10 ps and a production time at 300K of 50 ps. At the end of the dynamics run, the structure was again minimized to produce the final ATP/PMK complex. During the MD, motion was only

permitted for residues 120 to 160, which included the lid that contains R141. This approach to docking, with subsequent MD-based refinement, positioned ATP and M5P in their respective binding sites, is positions that are consistent with previous binding studies. In the end, there were no dramatic changes to the lid. Rather, there was mostly just an adjustment in the orientation of R141 sidechain, with modest lid rearanegement.

Protein Expression and Purification

PMK is normally a 192 residue 22.0 kDa protein, but it was expressed herein with an N-terminal histidine tag and additional linker residues, giving a total molecular weight of 24.2 kDa. Mutated PMK constructs (R84M, R111M, R130M, and R141M) were described previously.[8] Briefly, *E. coli* BL21-(DE3) Rosetta cells were transformed with a pET15b(+) expression construct of wild type and mutant PMK. The transformed cells were plated onto LB (Luria Bertani) agar plates containing ampicillin (amp) and chloramphenicol (chl). Plates were incubated overnight at 37 °C, and a single colony was picked to inoculate 2 mL of media, which was then grown to A_{600} ~ 0.3. This culture was then used to inoculate 20 LB-amp-chl plates. The plates were incubated overnight at 37 °C, and resulting bacterial lawns were used to inoculate 500 mL of M9 minimal media-amp-chl with $^{14}NH_4Cl$ and ^{13}C-glucose, as the sole sources of nitrogen and carbon, except media was supplemented with .25g/L [$^{13}C^6$, $^{15}N^4$]-L-Arginine (Isotec Inc.), to give A_{600} ~ 1.0. The liquid culture was then incubated at 30°C for 1 h prior to induction with 1 mM IPTG. The culture was harvested 4 h post induction at A_{600} ~2.0. Bacterial pellets were resuspended in 100 mL of a 50 mM KP_i (potassium phosphate) buffer containing 100 mM KCl, 5 mM imidazole, and 0.5 mM DTT at pH 7.8. Lysis was accomplished by passage through a microfluidizer at ~17 kpsi. The lysate was clarified by centrifugation

at ~100,000 g and the supernatant was loaded onto ~0.5-1.0 mL of Ni-Sepharose Fast Flow resin. The column was washed with lysis buffer until $A_{280} < 0.005$, and the protein was eluted with lysis buffer (stated above) supplemented with 300 mM imidazole. The fractions containing PMK were pooled and the concentration was determined spectrophotometrically using an extinction coefficient of $\epsilon_{280} = 32{,}290\ M^{-1}\ cm^{-1}$.

NMR Sample Preparation

All protein samples were buffer exchanged, using ultrafiltration with an Amicon (YM10) membrane, into 5 mM DTT, 20 mM KH_2PO_4, 10% D_2O, 10% d^6-glycerol, and 0.02% NaN_3, and concentrated to 400-600 μM. All experiments were performed at pH 6.5 and 298 K.

NMR Spectroscopy

All NMR experiments were performed on a 600 MHz Varian NMR System at 599.515 MHz using a triple resonance cryoprobe with z-axis gradients at 25 °C. Titrations were performed using 100 μM increments for M5P addition, until saturation was achieved based on ^1H-^{15}N HSQC chemical shift changes (1 mM for M5P). ^{15}N-T_1, ^{15}N-T_2, and $\{^1H\}$-^{15}N NOE experiments were all performed using the BioPack pulse sequences from Varian, Inc (Palo Alto, CA). Delay times for the T_1 experiments were 10.8, 108.3, 216.8, 379.2, 541.7, 758.4, 1083.4, 1516.8, and 2166.8 ms, and delay times for the T_2 experiments were 4.31, 8.62, 12.9, 17.2, 21.6, 30.2, 38.8, 47.4, 56.1 ms. T_1 experiments employed the standard inversion-recovery pulse sequence,[16] while T_2 experiments employed the CPMG sequence, as implemented previously.[17, 18] NOE's were obtained by measuring HSQC spectra with and without ^1H saturation for a time of 3

s (same for both), with an inter-scan delay of 1 sec. An interleaved approach was used for the T_1 and T_2 measurements, to decrease effects of field instability over long experiment times.[19, 20]

The 3D HNCO spectrum was acquired on the same 600 MHz instrument, using 16 transients, with 24 ^{13}C and 16 ^{15}N increments, using ^{13}C and ^{15}N spectral widths of 2250 and 1200 Hz, respectively. In addition to HNCO, we attempted CC(CO)NH and related TOCSY experiments, in an effort to obtain sidechain assignments, but very little TOCSY transfer was observed due to relaxation. A 3D HNCA was acquired using 16 transients, and 13 ^{13}C and 16^{15}N increments, with ^{13}C and ^{15}N spectral widths of 2100 and 1200 Hz, respectively. Processing of the 2D planes shown in Figures S4-5 was performed using 90° shifted sine bell window functions in ^{1}H and ^{15}N dimensions.

In an attempt to assign arginine sidechain NH's to backbone NH's, 3D ^{15}N-NOESY experiments were also acquired on apo-PMK with mixing times of 80 and 150 ms using 16 transients, with 70 ^{13}C and 79 ^{15}N increments, as shown in Figure S6. No assignments could be made using this experiment, as magnetization, when on the ε-NH, transferred rapidly to water and was subsequently destroyed with water suppression, which led to a decrease in signal intensity (red box in Figure S6) as compared to backbone NH intensity. Attempts to solve this issue using various forms of water suppression proved unsuccessful.

NMR Data Analysis

NMR data were processed using NMRPipe/NMRDraw,[21] and analyzed using NMRView.[22] For all experiments, ^{1}H-^{15}N spectra were processed using a 90° shifted sine function in the ^{1}H and ^{15}N dimensions. For ^{15}N-T_1 and ^{15}N-T_2 experiments, the spectra

with the shortest relaxation delay were peak picked using NMRView. For $\{^1H\}$-^{15}N NOE measurements only one spectrum was peak picked, and for each subsequent spectrum the peak ellipses were manually adjusted to fit each peak.

The R_1 and R_2 relaxation rates were determined by fitting the T_1 ($1/R_1$) and T_2 ($1/R_2$) curves to Equation 1:

$$I_t = I_o * e^{(-Rt)} \quad (1)$$

where I_t is the peak intensity after time t, I_o is the peak intensity at time t=0, and R is either R_1 or R_2. Fitting was done using the Rate Analysis package included in NMRView. NOE values were obtained by taking the ratio of the intensity versus the control. This was done with two sets of experiments in order to obtain an error for the analysis.

Modelfree Analysis

The parameters of internal motion were determined from the NMR relaxation data according to the model-free formalism established by Lipari and Szabo[23-25] using Modelfree4 software (version 4.20, A. G. Palmer, Columbia University). R_2/R_1 values were calculated for each complex for those assigned main chain residues and were used as the starting point for optimization of τ_c values. The optimized τ_c values (Table S1) were then fixed for each model afterward. Main chain and side chain dynamics calculations were performed with 300 Monte Carlo simulations per run using an internuclear N-H distance r_{NH} of 1.02 Å and a chemical shift anisotropy (CSA) for the ^{15}N nucleus of -172 ppm for backbone and -114 ppm for sidechain[13]. Five models were used to fit our experimental data and were iteratively tested in order of increasing complexity (M1= S^2; M2= S^2, τ_e; M3= S^2, R_{ex}; M4= S^2, R_{ex}, τ_e; M5= S^2_f, S^2_s, τ_e) until an acceptable fit was achieved. S^2 is the generalized order parameter, τ_e is the internal

correlation time, R_{ex} is the exchange contribution term, and S^2_f and S^2_s are for sub-nanosecond and nanosecond motions respectively. These models were tested until they could reproduce the experimental relaxation data within 90% confidence limits using appropriate χ^2 and F-tests. Sidechain N-H's predominantly fit to model 5 for apo-PMK, while the three ligand bound complexes fit best to model 4 in most cases.

To explore whether anisotropic rotation of PMK could be affecting the transverse relaxation of sidechain residues, thereby affected our S^2 calculations, we used our data from a previous dynamics study performed on the backbone NH's of PMK. In that study[4], we assessed ligand binding and dynamic properties of PMK, but there was no X-ray or NMR structure available (axial-anisotropic model needs a structure to optimize D_{ratio} for correlation time, which is the reason we could not use it in the current study of arginines as they are unassigned), so we could only use an isotropic model to assess correlation times of rotation (ns). Using the isotropic model and average R_2/R_1 as an initial estimate of τ_c, the correlation times were estimated for each complex (Table S3).

Table S3.

	Apo-PMK	M5P	MgADP	M5P/MgADP
τ_c (ns)	15.6	13.5	17.6	15.8

Now, to test whether anisotropic rotation could affect the correlation times of the previous study will (now that we have access to the crystal structure of human PMK), we will compare results using the axial model instead of the isotropic model. From the structure we have the calculated D_{ratio} for human PMK (0.88), giving it somewhat of a disc shape. This input, as well as the data from the previous study, gives us new estimated correlation times based on the anisotropic rotation of PMK (Table S4).

Table S4.

	Apo-PMK	M5P	MgADP	M5P/MgADP
τ_c (ns)	16.4	13.9	19.1	17.0

The S^2 values obtained from this new Modelfree analysis allowing anisotropic tumbling are nearly identical to the values reported in our previous study that assumed isotropic tumbling, validating that the use of the isotropic model in calculating the dynamic properties of PMK.

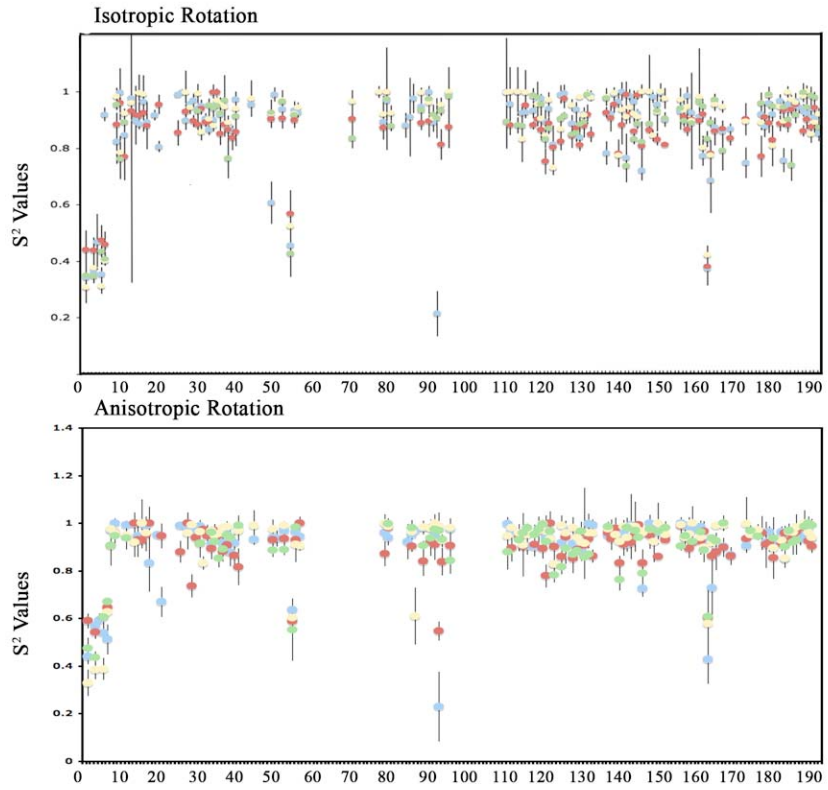

Figure S10. Comparison of S^2 values assuming isotropic versus anisotropic motion. Generally, there were not significant changes to S^2 values for backbone NH values. S^2 values assuming isotropic tumbling were from previously published work[4].

Chemical shift anisotropy values used were the typical -172 for the backbone NH's and -114 for the arginine sidechain NH's. The CSA for the sidechain NH's was selected based on previous literature (Trbovic, Nikola; Cho, Jae-Hyun; Abel, Robert; Friesner, R. A.; Rance, Mark; Palmer, A.,G. *J Am Chem Soc.* **2009**, *21*, 615-622)

Qualifying the Electrostatic Hypothesis

While the rigidification of arginine sidechains, due to binding of charge substrates to PMK, may well be due to electrostatic attraction over a long range, we realize that are data are only consistent with, but do not prove, such a causative relationship. But, to provide some evidence in favor of an electrostic hypothesis, we repeated the study of apo PMK and ADP-bound PMK, but now with the addition of 100 mM KCl. Interestingly, the higher salt concentration largely removed the ADP-induced rigidification of sidechains. This was unanticipated by us, as we felt the effect of salt would not be significant for longer range interactions, since dielectric of the protein might have been the main factor determining coulombic attractions. Perhaps the solvation of the distal surface arginine sidechains is the dominant factor (with dielectric of intervening protein of less importance). In any case, these results provide support that the order parameter increases, upon binding substrates, were electrostatic in nature. Also, it should be noted that while the apo PMK fit best to Model 5 in low salt, and the complexes fit best to Model 4 in low salt, we do not believe the increase in order parameter upon binding

substrate is due to going from model 5 to 4, because: (a) when we force a fit of apo PMK to Model 4, average S2 remains low (0.53, a small change from the original 0.49), (b) the Rex data that came from the Model 4 fit do not correlate with the order parameter changes (Fig. S10), and (c) at high salt both the apo and ADP-bound fit best to Model 5, yet both had low S2 values (Fig. S9).

Finally, we do not feel we are in a position to speculate on the functional importance (i.e. affinity for ligand; stabilization of protein) of the effects on arginine sidechain motion we report herein. Rather, we are just reporting that there is this interesting and previously unreported effect (i.e. side chain rigidification). We hope that our work will stimulate future studies, perhaps on simpler model systems, to better define the nature and role of the sidechain rigidification that we are observing.

References

(1) Mandel, A. M.; Akke, M.; Palmer, A. G.,3rd *J. Mol. Biol.* **1995**, *246*, 144-163.
(2) Clore, G. M.; Szabo, A.; Bax, A.; Kay, L. E.; Driscoll, P. C.; Gronenborn, A. M. *J. Am. Chem. Soc.* **1990**, *112*, 4989-4991.
(3) Kay, L. E.; Torchia, D. A.; Bax, A. *Biochemistry* **1989**, *28*, 8972-8979.
(4) Olson, A. L.; Yao, H.; Herdendorf, T. J.; Miziorko, H. M.; Hannongbua, S.; Saparpakorn, P.; Cai, S.; Sem, D. S. *Proteins* **2009**, 75, 127-138.
(5) Hellig, H., Popjak, G *J. Lipid Res.* **1961**, 235-243.
(6) Eyzaguirre, J.; Valdebenito, D.; Cardemil, E. *Arch Biochem Biophys.* **2006**, *454*, 189 196.
(7) Herdendorf, T. J.; Miziorko, H. M. *Biochemistry* **2006**, *45*, 3235-3242.
(8) Herdendorf, T. J.; Miziorko, H. M. *Biochemistry* **2007**, *46*, 11780-11788.
(9) Chang, Q.; Yan, X.; Gu, S.; Liu, J.; Liang, D. *Proteins* **2008**, *73*, 254-258.
(10) Buck, M.; Boyd, J.; Redfield, C.; MacKenzie, D. A.; Jeenes, D. J.; Archer, D. B.; Dobson, C. M. *Biochemistry* **1995**, *34*, 4041-4055.
(11) Cai, M.; Gong, Y. -.; Wen, L.; Krishnamoorthi, R. *Biochemistry* **2002**, *41*, 9572 9579.
(12) Hsu, S. T.; Cabrita, L. D.; Fucini, P.; Christodoulou, J.; Dobson, C. M. *J. Am. Chem. Soc.* **2009**, *131*, 8366-8367.
(13) Trbovic, Nikola; Cho, Jae-Hyun; Abel, Robert; Friesner, R. A.; Rance, Mark; Palmer, A.,G. *J Am Chem Soc.* **2009**, *21*, 615-622.
(14) Igumenova, T. I,. et al. *Chem. Rev.* **2006**, *106*, 1672-1699.

(15) Morris, G. M.; Goodsell, D. S.; Halliday, R. S.; Huey, R.; Hart, W. E.; Belew, R. K.; Olson, A. J. *J. Computational Chemistry* **1998**, *19*, 1639-1662.
(16) Teplyakov, A.; Sebastiao, P.; Obmolova, G.; Perrakis, A.; Brush, G. S.; Bessman, M. J.; Wilson, K. S. *EMBO J.* **1996**, *15*, 3487-3497.
(17) Farrow, N. A.; Muhandiram, R.; Singer, A. U.; Pascal, S. M.; Kay, C. M.; Gish, G.; Shoelson, S. E.; Pawson, T.; Forman-Kay, J. D.; Kay, L. E. *Biochemistry* **1994**, *33*, 5984-6003.
(18) Loria, J. P.; Rance, M.; Palmer, A. G. *J. Am. Chem. Soc.* **1999**, *121*, 2331-2332.
(19) Zhu, G.; Xia, Y.; Nicholson, L. K.; Sze, K. H. *J. Magn. Reson.* **2000**, *143*, 423-426.
(20) Gagne, S. M.; Tsuda, S.; Spyracopoulos, L.; Kay, L. E.; Sykes, B. D. *J. Mol. Biol.* **1998**, *278*, 667-686.
(21) Tjandra, N.; Wingfield, P.; Stahl, S.; Bax, A. *J. Biomol. NMR* **1996**, *8*, 273-284.
(22) Delaglio, F.; Grzesiek, S.; Vuister, G. W.; Zhu, G.; Pfeifer, J.; Bax, A. *J. Biomol. NMR* **1995**, *6*, 277-93.
(23) Johnson, B. A., and Blevins, R. A. *J. Biomol. NMR* **1994**, 603-614.
(24) Lipari, G.; Szabo, A. *J. Am. Chem. Soc.* **1982**, *104*, 4546-4559.
(25) Lipari, G.; Szabo, A. *J. Am. Chem. Soc.* **1982**, *104*, 4559-4570.
(26) Clore, G. M.; Szabo, A.; Bax, A.; Kay, L. E.; Driscoll, P. C.; Gronenborn, A. M. *J. Am. Chem. Soc.* **1990**, *112*, 4989-4991.